

Coated Stainless Steel Bipolar Plates for Proton Exchange Membrane Electrolyzers

To cite this article: P. Lettenmeier *et al* 2016 *J. Electrochem. Soc.* **163** F3119

View the [article online](#) for updates and enhancements.

You may also like

- [Bulk Aging of Graphite-Polypropylene Current Collectors Induced by Electrochemical Cycling in the Positive Electrolyte of Vanadium Redox Flow Batteries](#)
Barbara Satola, Lidiya Komsiyyska and Gunther Wittstock
- [Performance and Limitations of 3D-Printed Bipolar Plates in Fuel Cells](#)
Benjamin D. Gould, Joseph A. Rodgers, Michael Schuette *et al.*
- [Electrochemical Aging and Characterization of Graphite-Polymer Based Composite Bipolar Plates for Vanadium Redox Flow Batteries](#)
Gaurav Gupta, Barbara Satola, Lidiya Komsiyyska *et al.*



245th ECS Meeting • May 26-30, 2024 • San Francisco, CA

Present your work at the leading electrochemistry & solid-state science conference.

Network with academic, government, and industry influencers!

Submit abstracts by December 1, 2023

[Learn more & submit!](#)





Coated Stainless Steel Bipolar Plates for Proton Exchange Membrane Electrolyzers

P. Lettenmeier,^a R. Wang,^b R. Abouatallah,^b F. Burggraf,^a A. S. Gago,^{a,z}
and K. A. Friedrich^{a,c,*}

^aInstitute of Engineering Thermodynamics, German Aerospace Center, Stuttgart 70569, Germany

^bHydrogenics Corporation, Mississauga, ON L5T 2N6, Canada

^cInstitute of Energy Storage, University of Stuttgart, Stuttgart 70550, Germany

Given its rapid response to fluctuating currents and wide operation range, proton exchange membrane (PEM) water electrolysis is utmost suitable for generation of hydrogen from renewable power. However, it is still hindered by the high cost of the stack components compared to those used in the alkaline technology. In particular, the titanium bipolar plates (BPP) are an issue and the replacement of this metal by stainless steel is a challenge, due to the highly corrosive environment inside PEM electrolyzer stack. Herein, we coat stainless steel BPPs with 50–60 μm Ti and 1.5 μm Pt coatings by vacuum plasma spraying (VPS) and magnetron sputtering physical vapor deposition (PVD), respectively. The BPPs are evaluated at constant 1 A cm^{-2} for more than 1000 h. The thermally sprayed Ti coatings fully protect the stainless steel substrate during this period of time, and the Pt surface modification allows achieving a cell performance comparable to the baseline.

© 2016 The Electrochemical Society. [DOI: 10.1149/2.0141611jes] All rights reserved.

Manuscript submitted April 19, 2016; revised manuscript received June 8, 2016. Published July 21, 2016. *This paper is part of the JES Focus Issue on Electrolysis for Increased Renewable Energy Penetration.*

In 1800, William Nicholson and Anthony Carlisle discovered the electrolysis of water into H_2 and O_2 , by applying direct current (DC) and for a long time it was the main technique for the hydrogen production for industry.¹ Over 200 years later, the splitting of water is experiencing a renaissance due to energy applications and proton exchange membrane (PEM) electrolysis is the most dynamic technique, which was reported in 1973 by Russell and coworkers.² In this context, hydrogen is nowadays expected to act as a carbon neutral energy vector to introduce renewable electricity into other sectors.³ Compared to the well-established alkaline technology, PEM electrolyzers have several advantages such as high efficiency, rapid response, compact system design, and extended dynamic operation range.^{4–9} Moreover, gas purities up to 99.995% can be achieved with the PEM technology while only 99.5% for alkaline electrolyzers.¹⁰ Conversely, for small production rate, PEM technology is more expensive than alkaline.^{11,12} However, it becomes more competitive and likely cheaper in large production rates, especially in the Megawatt input power range.

The stack, which is assembled with several cells connected in series, is the key part of the PEM electrolyzer unit.⁶ The membrane electrode assembly (MEA) is one core component of a PEM cell. Current collectors (CC) on both sides of the MEA, which are permeable to water and the product gases, allow current to flow to and from the electrodes.^{13–15} The two half-cells are surrounded by so called bipolar plates (BPP) or separators, which usually have flow fields that allow the reactant water to be transported to the CC and the product gases to be removed efficiently.^{16,17}

The stack comprises about 60% of the total cost of the PEM electrolyzer and the titanium bipolar plates (BPP) are responsible for half the cost of the stack.⁸ The BPPs are manufactured from titanium, which is highly stable to corrosion in oxidative environments, but machining this metal is complicated and expensive.^{18,19} Furthermore, semi-conductive oxides form on its surface as a result of anodization and they affect negatively the performance and durability of the electrolyzer.^{20–23} Thereby, the reduction or total replacement of massive Ti in PEM electrolyzers by low cost materials is a pressing issue for the industry.

The use of stainless steel as base material for manufacturing BPPs of proton exchange membrane fuel cell (PEMFC) has been extensively reported. When used in fuel cells, it requires a high corrosion resistance coating with excellent electronic properties.^{24–26} In this context, conductive coatings such as C,^{27–29} Au,³⁰ TiN,³¹ TiN/C,³² TaN,³³

CrN,³⁴ and $\text{SnO}_2\text{:F}$ ³⁵ have been extensively evaluated for corrosion protection of PEMFC stainless steel bipolar plates. Nevertheless, these coated-BPPs are not currently used in PEM electrolyzers. The reason is that the high cell voltage, at which the electrolyzer operates in nominal conditions (2 V, 40–60°C, 1×10^5 Pa or higher), accelerates corrosion, which might not be avoided with PEMFC coatings.

An approach for developing protective coatings for BPPs of PEM electrolyzers can be: (i) Deposition of a thick Ti coating by thermal spraying^{36–40} for corrosion protection of stainless steel; (ii) Surface modification of the Ti coating to decrease contact resistance.^{21,41,42} We have recently shown that a coating of Ti with a subsequent surface modification with Pt (Pt/Ti) protects stainless steel from corrosion over an extended period of time, while maintaining its electrical properties.³⁹ In our work the corrosion evaluation was performed in a simulated environment of PEM electrolyzer for short periods. However, long-term testing of the coatings in a commercial PEM electrolyzer is crucial to demonstrate their capability for industrial applications. In this work, we report the results of a 1000 h test on a stack with Ti and Pt/Ti coated stainless steel bipolar plates in a commercial PEM electrolyzer. Neither decrease in the electrolyzer performance nor degradation of the stainless steel substrate was observed, proving that this metal can be used as base material for manufacturing low cost bipolar plates.

Experimental

Coating process and stack assembly.—The development of the Ti and Pt coatings on stainless steel was reported elsewhere.³⁹ The coatings were deposited on 120 cm^2 active area 316L stainless steel round BPP from Hydrogenics. The plates were previously sand-blasted with SiO_2 powder to increase the surface roughness of the support thus the adherence of the Ti coating to it is improved. A feedstock of titanium powder (grade 1, grain size < 45 μm , TLS Technik Spezialpulver) was used. The coating was applied on both sides of the plates. The chamber pressure was 50 mbar. A plasma enthalpy of 21.3 MJ kg^{-1} was achieved by carefully controlling the flow rates of H_2 , He and Ar. The presence of H_2 decreases the partial pressure of O_2 and its reduction by H_2 takes place, thus preventing the oxidation of Ti into TiO_2 . The former increases the electrical resistance of the Ti coating. Thereafter, a step of capillary sealing procedure allowed to fully densify the Ti coatings. Finally, the area of the flow field that is in contact with the current collectors was sanded with SC4000 paper and rinsed with deionized (DI) water. No abrasives were used. An additional layer of Pt was deposited on some of the Ti-coated stainless steel BPP,

*Electrochemical Society Member.

^zE-mail: aldo.gago@dlr.de

Table I. Arrangement of coated stainless steel (ss) bipolar plates in the stack.

Cell	Anode bipolar plate	Cathode bipolar plate
1	Baseline ^a	Baseline ^a
2	Baseline ^a	Baseline ^a
3	Ti/ss	Baseline ^a
4	Ti/ss	Ti/ss
5	Pt/Ti/ss	Ti/ss
6	Pt/Ti/ss	Pt/Ti/ss

^aCoated titanium bipolar plate. The coating (non-disclosed) is proprietary technology of Hydrogenics.

by magnetron sputtering physical vapor deposition (PVD). The BPP were assembled in a rainbow stack and in which all cells had the same commercial membrane electrode assemblies MEAs (Greenerity E300, N115CS membrane), metallic current collectors and carbon-based gas diffusion layers (GDL). Table I enlists the configuration of the cell coatings in the stack. The first two cells, which had Ti bipolar plates with proprietary coatings from Hydrogenics, were used as a baseline for comparison purposes.

PEM electrolyzer and impedance tests.—The stack (model 92E, Hydrogenics), Figure 1a, with coated stainless steel bipolar plates was tested in a commercial PEM electrolyzer (0.75–2.5 Nm³ H₂ h^{−1} “Hylyzer” Hydrogen Generator, Hydrogenics), Figure 1b. The electrolyzer was running for several days as part of an activation protocol until it reached a stable voltage at a given current density. Then the stack was evaluated at constant 1 A cm^{−2}, for 1000 h, at 38°C, and 6.5 × 10⁵ Pa balanced pressure system. This current density was deliberately chosen to compare degradation rates with other reports, in which PEM electrolyzers with Ti BPP were operated at least 100 h.^{18,43–46} Polariza-

tion curves were recorded before, and after 500 and 1000 h, from 0.01 to 1 A cm^{−2} (rectifier step rate: 4.2 mA cm^{−2} s^{−1}) at 29°C and 6.5 × 10⁵ Pa balanced pressure system. Temperature fluctuations were negligible in this current density range. Likewise, electrochemical impedance spectroscopy (EIS) measurements were carried out with a potentiostat/galvanostat (Zahner elektrik IM6) coupled with a booster (Module PP240) for each cell at 27°C. Measurements were carried out at 20 A with an amplitude of 3 A and frequencies between 0.1 and 750 Hz. The results were fitted to an equivalent electrical circuit consisting of an ohmic resistance (R₁) connected in series with two sections of resistance - constant phase element (R₂-CPE, R₃-CPE). The first element, R₁, represents the ohmic behaving components of the cell, containing electrical and ionic resistances. The second component, R₂-CPE, represents capacitive double layer effects in the electrode of ionic and electric components, and the third component, R₃-CPE, corresponds to the charge transfer resistance of the oxygen evolution reaction.

The inlet water resistance of the stack was kept higher than 10 MΩ cm^{−1} at all time, by means of a DI water resin system, which traps transition metal ions as well as S, F and Si. Therefore, the resin can be used to determine qualitatively stack degradation products from catalysts and coatings. X-ray photon electron spectroscopy (XPS) was performed at the end of the 1000 h test looking for Fe or other elements of the 316L.

Contact resistance measurements.—Interfacial contact resistance (ICR) vs. compaction force measurements were performed after the 1000 h test to evaluate degradation effects due to formation of semi-conducting oxide layers on the surface of the coatings. This technique is widely used to determine ICR of BBP for PEMFC.^{32,35,47–49} We assume that the ICR parameter of the coated stainless steel BPP before the test is similar to the one determined on Ti and Pt/Ti coated dummy flat samples,³⁹ since the coating parameters in this work were

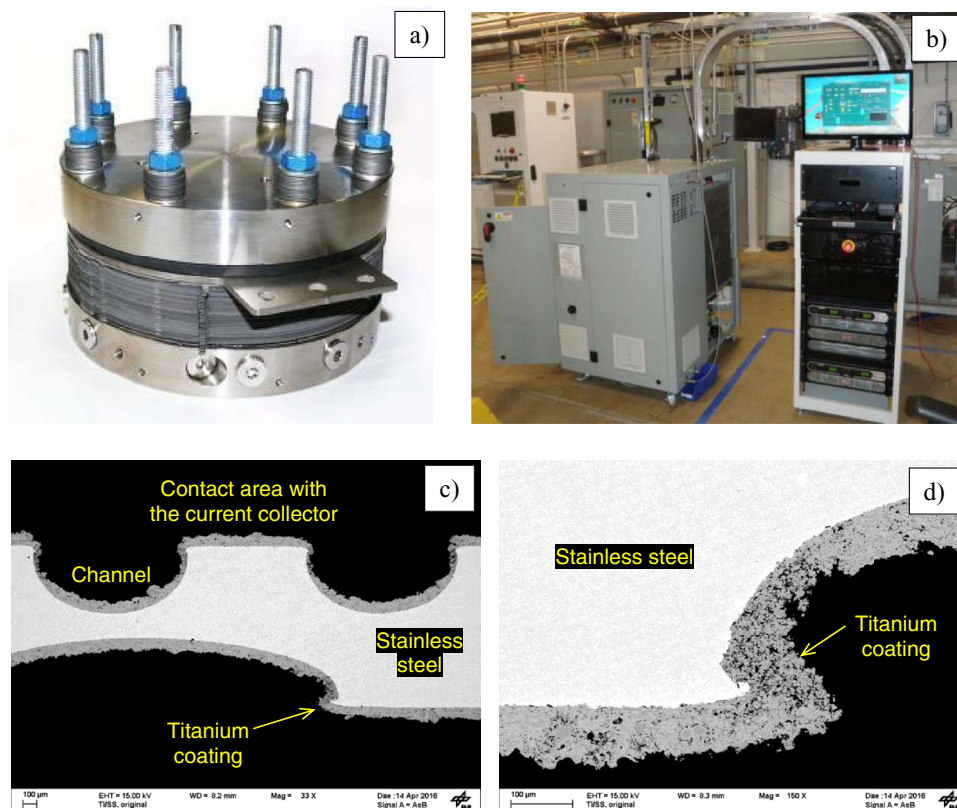


Figure 1. a) Stack (E92, Hydrogenics) 120 cm² 6-cell stack tested in b) a 0.75–2.5 Nm³ H₂ h^{−1} “Hylyzer” PEM electrolyzer unit (Hydrogenics); c) Cross-section SEM image of a Ti-coated stainless steel bipolar plate before sanding; d) Cutaway of a corner between the channel of the flow field and contact area with the current collector.

the same. The bipolar plates were placed between two pieces of GDL carbon paper (280 μm thick) and two copper cylinders, which were previously cleaned with 0.5 M H_2SO_4 . The ICR measurements were performed by applying a current of 5 A and the contact pressure was varied from 20 to 200 N cm^{-2} . The separation between the channel ribs and width of the rib is in both cases ~ 1 mm after coating. Therefore, the compaction force was adjusted by a factor of two. The voltage was measured with the same potentiostat used for the EIS measurements. An electrical circuit, which represents each interface by a resistor,⁴⁹ was used to determine the ICR of each plate.

Scanning electron microscopy (SEM).—Analysis of the cross section of the coated-BPPs was carried with an ULTRA plus (Zeiss Corp.) scanning electron microscope. The images were recorded with the secondary electrons an integrated AsB GEMINI lens detector, separating the back scattered electron (BSE) signal. The acceleration voltage was 15 kV and the working distance 8.1 mm.

Discussion of Results

Coated stainless steel BPP.—One concern of every coating procedure is how well the layer can cover zones in the BPPs that are more prone to corrosion than others. Cross-section SEM images of the Ti-coated stainless steel BPPs, readily after being coated are presented in Figures 1c and 1d. The micrographs reveal that the coating covers all the regions of the manifolds, the exposed 3D areas of the flow field, inlet/outlet holes, edges, corners and even some regions of the back side of the BPP. It is worthwhile noting that it was not necessary to tilt the plate to obtain a uniform thickness of the coating on all the surface of the ribs of the BPP. The BPP with Pt/Ti coatings were not analyzed by SEM prior the assembly of the stack, assuming that the morphology of the coatings is similar coatings reported elsewhere.³⁹

Cell performance.—The 92E stack with the coated-BPPs was mounted in the Hylyzer PEM electrolyzer and operated for a few days as part of an activation process. Thereafter, current-voltage curves from 0.01 to 1 A cm^{-2} were recorded for each cell at a rectifier step rate of 4.2 $\text{mA cm}^{-2} \text{ s}^{-1}$, maintaining a stack temperature of 29°C, Figure 2a. According to the cell configurations presented in Table 1, the cells with Ti-coated cathodes without Pt, cell 4 and 5, showed the highest E_{cell} at 1 A cm^{-2} . The Nyquist plots of the EIS measurements at 27°C and 0.166 A cm^{-2} are presented in Figure 2b. It needs to be mentioned, that the E_{cell} of the baseline and the Pt/Ti coated cells at 38°C is high compared to what it has been reported with same stack technology.⁵⁰ The issue can originate from an increase of water pressure in the flow field channels and sealing compression in the grooves caused by the thick Ti coating, which affected the performance of the whole stack. Consequently, the width of the flow field channels and sealing grooves should be adjusted if they are to be coated with 50–60 μm Ti. As a result, our study can only compare the performance of the Pt/Ti coated cells with the baseline in the same stack. Further work will address this issue.

First, the EIS results show that cell 4 and 5 have much higher ohmic resistance (R_1) compared to the others. As it will be shown in the next section, the ICR of the Ti coating with the carbon-based GDL is much higher than the ICR of the Pt coating with the same GDL. One can conclude that the passivation of Ti is detrimental for the cell performance when using a carbon based GDL in the cathode. Indeed, a significant improvement in the performance of unitized reversible fuel cells (URFC) has been previously reported, when the Ti bipolar plates are coated with Pt²¹ or Au.⁴² Second, the kinetic or activation resistance (R_3) is similar in all cells, since they all have MEAs with similar catalysts. None of the cells presented mass transport issues, which accounts for an excellent gas bubble management in the catalyst layers,⁵¹ thin current collectors with high porosity^{13,52,53} and optimized flow field of the bipolar plate.¹⁶ Lastly, cell 6, having Pt/Ti coating on anode and cathode side of the stainless steel BPP, showed the lowest E_{cell} at 1 A cm^{-2} .

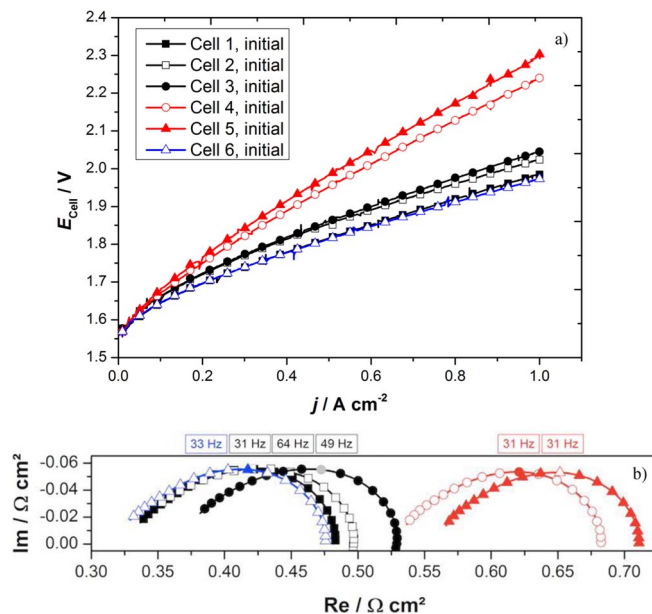


Figure 2. a) Initial current-potential curves of cell 1–6 from 0.01 to 1 A cm^{-2} and a scanning rate of 4.2 $\text{mA cm}^{-2} \text{ s}^{-1}$, 29°C and balanced pressure system of 6.5×10^5 Pa; b) Nyquist plot of the initial EIS measurement at 27°C, 0.166 A cm^{-2} and an amplitude current of 3 A. The apex of the frequency is indicated on top.

A 1000 h test at 1 A cm^{-2} was carried out readily after the initial electrochemical characterization of the stack. The resulting E_{cell} vs. time characteristics of cell 1–6 are presented in Figure 3. The electrolyzer was shut down after ~ 500 h of operation and it was kept in this mode for almost 100 h to determine degradation effects when the electrolyzer is turned off. These conditions will necessarily occur in any application when H_2 is not constantly required. Current potential curves and EIS were recorded at the end of the stand-by period, Figures 4a and 4b. Once the electrolyzer was brought back in operation, the voltage of cell 4 and 5 was more than 100 mV higher than before the shutting down, while for the other four cells such changes did not occur. By fitting the equivalent circuit proposed in PEM electrolyzer and impedance tests section, the changes of the ohmic resistances of each cell can be quantified. The ohmic resistance of the surface modified cells decreases almost homogeneously by an average value of 45 $\text{m}\Omega \text{ cm}^{-2}$. Conversely, cell 4 and cell 5 increased their ohmic

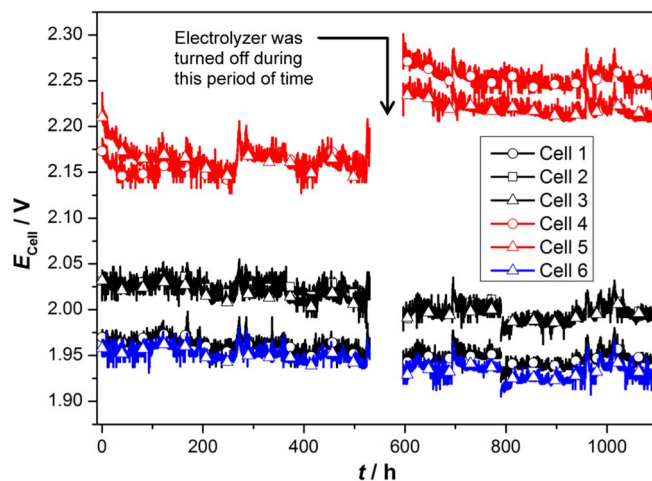


Figure 3. Cell potential (E_{cell}) during the 1000 h test on cell 1–6 at 1 A cm^{-2} , at 38°C and balanced pressure system of 6.5×10^5 Pa.

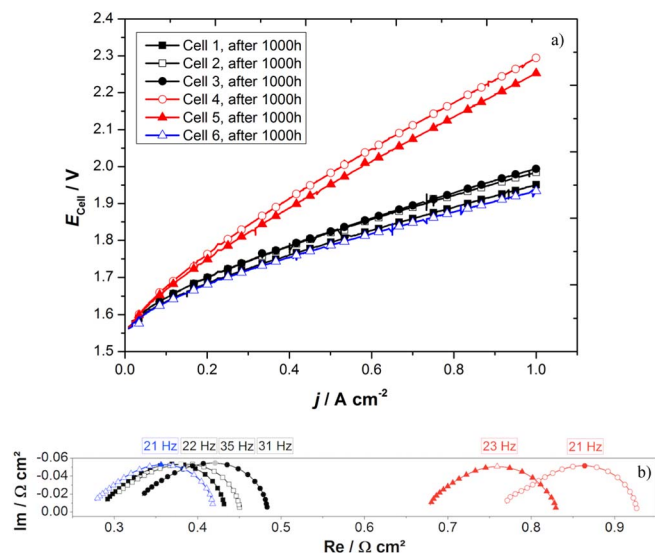


Figure 4. a) Current-potential curves of cell 1 to cell 6 from 0 to 1 A cm^{-2} and at 29°C after 1000 h test at constant 1 A cm^{-2} ; b) Nyquist plot of the EIS measurement at 27°C , 0.166 A cm^{-2} and an amplitude current of 3 A after 1000 h constant operation at 1 A cm^{-2} . The apex of the frequency is indicated on top.

resistance by 243 and $117 \text{ m}\Omega \text{ cm}^{-2}$, respectively. Post-mortem analysis (Degradation and post-mortem analysis section) will show that not only the anode side of the Ti coated plate oxidized, but also the cathode side experienced degradation. The negative effect might have occurred during the stand-by period as concluded from the time equivalence of degradation and stand-by period, although it was not directly proven.

The change of E_{cell} and R_1 for all the cells is summarized in Figures 5a and 5b, respectively. In overall, cell 1 (baseline) and cell 6 (Pt/Ti coating on anode and cathode) showed the highest performance and no increase in E_{cell} . The main difference between them is that cell 1 is made of Ti, while cell 6 uses stainless steel as based material for its manufacture. Except for cell 4, the performance of the cells improved slightly overtime, which can be explained by a progressive decrease of the ohmic (R_1), Figure 5b. Cell 4 and cell 5 improve significantly their performance in the initial 100 h until reaching a steady state. From Figure 3 one can only observe the improvement of their performance in the initial 100 h, which is a complex activation process (recovering) not yet fully explored in the literature of PEM electrolysis. Both cells progressively continue degrading and in particular after the shut down period, which can be well appreciated from Figure 5a (Increase in E_{cell}) and Figure 5b (increase in R_1). The performance of both cells did not recover anymore for the subsequent 900 h. From the polarization curves of Figures 2a and 4a (as well as in Figure 5b: high increase in R_1) one can observe that cell 4 degraded more than Cell 5 after the 1000 h test.

Moreover, other works have reported a concomitant increase in E_{cell} has as result of degradation^{18,43–46} and the cause is mostly attributed to poisoning of the MEA with metallic cations such as Fe.^{54–57} This metal is present in the DI water in small amounts and it increases its concentration over time in the O_2 separator due to the electrolysis process. Therefore, a DI water resin is necessary for trapping the Fe ions and it needs to be replaced regularly. The effect of Fe poisoning in PEM electrolyzers is not well studied so far but it is expected that Fe will decrease the ionic conductivity and deposit on the cathode.⁵⁸ As a result, the E_{cell} will increase over time. In our study, we did neither observe rise of E_{cell} of the cells with Pt/Ti/ss bipolar plates nor abnormal increase of iron concentration in the DI water resin, and nor pitting corrosion after the 1000 h test.

From the results discussed in this section, it can be concluded the following: (i) The titanium coating does not need further surface mod-

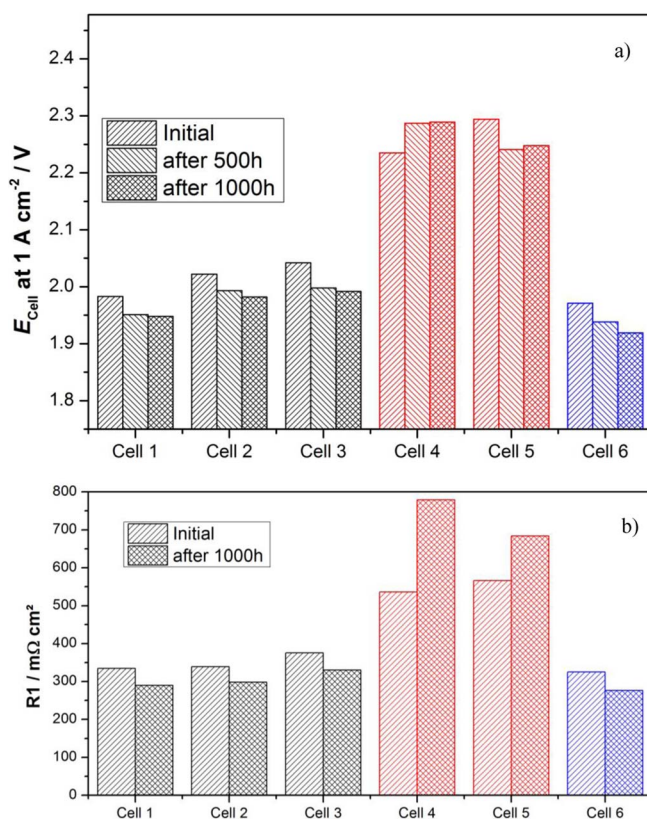


Figure 5. a) Cell potential of cell 1 to cell 6 at 1 A cm^{-2} , 29°C , $6.5 \times 10^5 \text{ Pa}$ and at three time steps, initial, after 500 h and after 1000 h constant performance at 1 A cm^{-2} ; b) Initial ohmic resistance (R_1) of cell 1 to cell 6 and after 1000 h constant performance at 1 A cm^{-2} at 27°C .

ification on the anode side if it is in contact with a metallic collector; (ii) The titanium coating should be modified, with Pt for example, if carbon paper GDL is to be used as cathode current collector; (iii) The stainless steel BPP might not require a Ti coating on the cathode side. Further investigations are necessary in order to demonstrate (iii), as corrosion of stainless steel might occur in the periods when the electrolyzer is turned off.

Degradation and post-mortem analysis.—After disassembling of the stack, a noticeable darkness of the surface of the Ti coating in the cathode and anode side of the plate was observed. The grayish surface of the coating on the anode side reappeared after sanding it for a few minutes with SC4000 paper, thus removing the oxide layer. The ICR vs. compaction force measurements were carried on areas of the BPP before and after sanding procedure to evaluate the effect of degradation. Figure 6 summarizes the results on Ti/ss while Pt/Ti/ss is included for comparison. First, one can observe that the Pt surface modification reduces the contact resistance of Ti with the carbon paper almost 2 orders of magnitude at 120 N cm^{-2} and does not change with the compaction pressure, which was already observed in our previous work.³⁹

Secondly, the surface of the cathode degraded more than the anode side. If the cause was oxidation of the Ti coating, certainly, it did not take place during operation of the electrolyzer, but most likely during the stand-by period in which the electrolyzer was turned off. One must also consider the possibility of degradation of the cathode Ti coating by H_2 embrittlement.^{59,60} The results of ICR vs. compaction force suggest that the cathode side might not necessarily need to be coated with Ti as austenitic stainless steels are more resistant to hydrogen embrittlement.^{61,62} In the case of the Pt/Ti-coated stainless steel BPP, the Pt coating peeled off in some areas of the grooves of the BPP in which the sealing is inserted. However, no signs of degradation

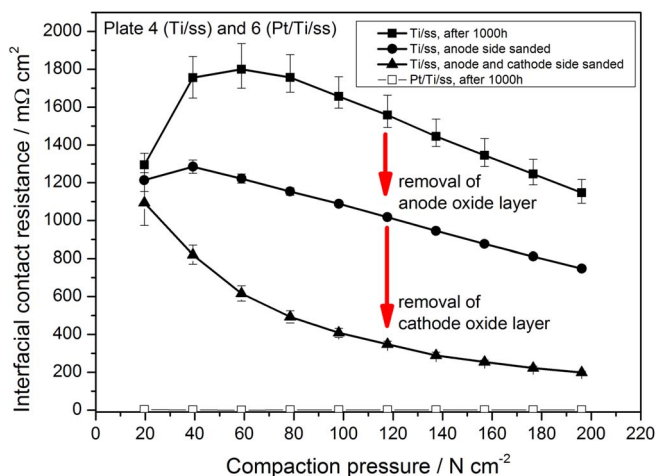


Figure 6. Interface contact resistance (ICR) with respect of compaction pressure of plate 4 (Ti/ss) and plate 6 (Pt/Ti/ss) after 1000 h constant performance at 1 A cm⁻² at 38°C. The anode and cathode sides of the Ti/ss BPP were sanded to remove any oxide layer.

Table II. XPS analysis of the DI water resin in the anode cycle of the PEM electrolyzer system before (fresh) and after (used) 1000 h constant performance at 1 A cm⁻².

Element	Fresh [wt%]	Used [wt%]
O	10.9	18.5
C	79.6	72.9
S	7.2	6.2
Si	0	1.8
Fe	0	0.1
Ti	0	0.3
Ir	0	0.2
N	2.4	-

of the Pt coating were observed in the contact area with either the metallic CC (anode) or carbon-based GDL (cathode). The peeling of the thermally sprayed Ti coating was neither observed for the Ti/ss nor Pt/Ti/ss BPPs.

Samples of the DI water resin were collected at the beginning (fresh) and the end (used) of the 1000 h and they were analyzed by X-ray photon electron microscopy (XPS). Table II enlists the elements that were detected, and in particular Ti and Fe concentration in the resin increased by 0.3 and 0.1 wt%, respectively, after the 1000 h test. The former might originate in the degradation of the Ti BPPs (cell 1–2) or the Ti coating (cell 3–4). Yet, the element of interest is iron, which is a product of pitting corrosion of stainless steel. The increase of this metal in the resin is negligible and even higher amounts have been

observed for other E92 stacks having only Ti BPPs (measurements not shown). Therefore, the traces of Fe in the resin can only arise from inlet water for the entire system, as corrosion of stainless 316L steel pipes and valves in DI water is unlikely.⁶³ Finally, Figure 7a shows a SEM cross-section of optical image of the Ti coating on the stainless steel BPPs after the 1000 h test. A close up image of the Pt/Ti coating deposited on the anode side of the BPP is presented on in Figure 7b. Neither peeling off the coatings nor corrosion of the substrate (pinholes) was observed in any plate. The electrochemical and post-mortem physical analysis clearly support the use of stainless steel as base material for BPPs of PEM electrolyzers.

Conclusions

Thermally sprayed Ti-coated stainless steel bipolar plates of PEM electrolyzer were tested for more than 1000 h at constant 1 A cm⁻². The coating fully protected the stainless steel substrate; however it degraded when used in the cathode and in contact with the carbon-based GDL, resulting in a significant increase of cell voltage (E_{cell}). The oxidation of the Ti coating on the anode side did not pose a negative effect. The problem was solved by modifying the surface of the Ti coating with a 1.5 μm Pt layer (Pt/Ti). The highest performance of the PEM electrolyzer was achieved with this dual coating deposited on the anode and cathode side. Additional results suggest that no coating is necessary on the cathode side, if stainless steel is to be used as base material for manufacturing the BPPs. Furthermore, cheaper steels, Cu, or Al can possibly be used instead of stainless steel since corrosion was not observed. However, the BPP made of these metals would require a coating on both sides to protect against any possible corrosion phenomena, in particular during the stand-by periods.

Acknowledgments

The authors are deeply grateful to the Federal Ministry for Economic Affairs and Energy (BMWi), project No. 0325440A, and the internal funding program: Helmholtz association (HGF), POF III for financial support. We also thank Anke Steinhilber for XPS analysis, Ina Plock for the SEM images, and Svenja Kolb, Jörg Bürkle for their technical support in the electrochemical measurements.

References

- Royal Society of Chemistry, *Chem. World*, 2003, *Enterp. electrolysis* (2003).
- J. H. Russell, L. J. Nuttall, and A. P. Fickett, *Am. Chem. Soc. Div. Fuel Chem. Prepr.*, **18**, 24 (1973).
- A. Sternberg et al., *Energy Environ. Sci.*, **8**, 389 (2015).
- K. E. Ayers, C. Capuano, and E. B. Anderson, *ECS Trans.*, **41**, 15 (2012).
- K. E. Ayers, L. Moulthrop, and E. B. Anderson, *ECS Trans.*, **41**, 75 (2012).
- M. Carmo, D. L. Fritz, J. Mergel, and D. Stolten, *Int. J. Hydrogen Energy*, **38**, 4901 (2013).
- F. Barbir, *Sol. Energy*, **78**, 661 (2005).
- L. Bertuccioli et al., *Study on development of water electrolysis in the EU by E4tech Särl with Element Energy Ltd for the Fuel Cells and Hydrogen Joint Undertaking* (2014).

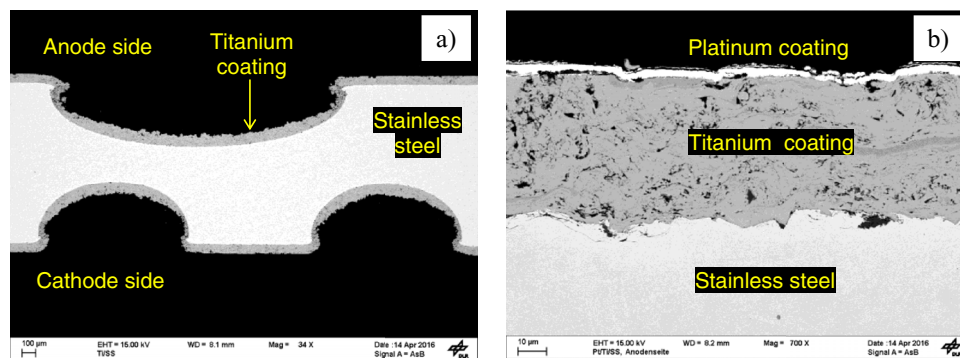


Figure 7. Post-mortem cross-section SEM images a) Ti and b) Pt/Ti coatings on stainless steel BPPs after the 1000 h test at constant 1 A cm⁻².

9. K. E. Ayers et al., *ECS Trans.*, **33**, 3 (2010).
10. K. Zeng and D. Zhang, *Prog. Energy Combust. Sci.*, **36**, 307 (2010).
11. Fuel Cells and Hydrogen Joint Undertaking, *Commercialisation of energy storage in europe, A fact-based analysis of the implications of projected development of the European electric power system toward 2030 and beyond for the role and commercial viability of energy storage*, p. 52 (2015).
12. K. A. Friedrich, *Studie über die Planung einer Demonstrationsanlage zur Wasserstoff - Kraftstoffgewinnung durch Elektrolyse mit Zwischenspeicherung in Salzkavernen* (2015).
13. S. A. Grigoriev, P. Millet, S. A. Volobuev, and V. N. Fateev, *Int. J. Hydrogen Energy*, **34**, 4968 (2009).
14. H. Ito et al., *Int. J. Hydrogen Energy*, **37**, 7418 (2012).
15. M. A. Hoeh et al., *Electrochem. commun.*, **55**, 55 (2015).
16. H. Ito et al., *Int. J. Hydrogen Energy*, **35**, 9550 (2010).
17. A. S. Tijani, D. Barr, and A. H. A. Rahim, *Energy Procedia*, **79**, 195 (2015).
18. H. G. Kim, L. K. Kwa, W. Han, L. K. Kwac, and W. Han, in *International Conference on Power and Energy Systems Lecture Notes in Information Technology*, vol. **13**, p. 373 (2012).
19. C. K. Jin, M. G. Jeong, and C. G. Kang, *Int. J. Hydrogen Energy*, **1** (2014).
20. J.-T. T. Wang, W.-W. W. Wang, C. Wang, and Z.-Q. Q. Mao, *Int. J. Hydrogen Energy*, **37**, 12069 (2012).
21. H.-Y. Jung, S.-Y. Huang, and B. N. Popov, *J. Power Sources*, **195**, 1950 (2010).
22. S. S. Dhrab, K. Sopian, M. A. Alghoul, and M. Y. Sulaiman, *Renew. Sustain. Energy Rev.*, **13**, 1663 (2009).
23. D. R. Hodgson, B. May, P. L. Adcock, and D. P. Davies, *J. Power Sources*, **96**, 233 (2001).
24. R. A. Antunes, M. C. L. Oliveira, G. Ett, and V. Ett, *Int. J. Hydrogen Energy*, **35**, 3632 (2010).
25. M. C. L. de Oliveira, G. Ett, and R. A. Antunes, *J. Power Sources*, **206**, 3 (2012).
26. L. Peng, P. Yi, and X. Lai, *Int. J. Hydrogen Energy*, **39**, 21127 (2014).
27. H. Husby, O. E. Kongstein, A. Oedegaard, and F. Seland, *Int. J. Hydrogen Energy*, **39**, 951 (2014).
28. W. J. Pech-Rodríguez, D. González-Quijano, G. Vargas-Gutiérrez, and F. J. Rodríguez-Varela, *Int. J. Hydrogen Energy*, **39**, 16740 (2014).
29. Z. Wang et al., *Int. J. Hydrogen Energy*, **41**, 5783 (2016).
30. A. Kumar, M. Ricketts, and S. Hirano, *J. Power Sources*, **195**, 1401 (2010).
31. Y. Wang and D. O. Northwood, *J. Power Sources*, **191**, 483 (2009).
32. H. Sun, K. Cooke, G. Eitzinger, P. Hamilton, and B. Pollet, *Thin Solid Films*, **528**, 199 (2013).
33. C. Choe, H. Choi, W. Hong, and J.-J. Lee, *Int. J. Hydrogen Energy*, **37**, 405 (2012).
34. Y.-C. Park et al., *Int. J. Hydrogen Energy*, **38**, 10567 (2013).
35. H. Wang and J. A. Turner, *J. Power Sources*, **170**, 387 (2007).
36. J. Kawakita et al., *Surf. Coatings Technol.*, **201**, 1250 (2006).
37. T. Valente and F. P. Galliano, *Surf. Coatings Technol.*, **127**, 86 (2000).
38. H. Ji and P. M. Marquis, *Surf. Coatings Technol.*, **45**, 121 (1991).
39. A. S. Gago et al., *J. Power Sources*, **307**, 815 (2016).
40. A. S. Gago et al., *ECS Trans.*, **64**, 1039 (2014).
41. T. J. Toops et al., *J. Power Sources*, **272**, 954 (2014).
42. H.-Y. Jung, S.-Y. Huang, P. Ganesan, and B. N. Popov, *J. Power Sources*, **194**, 972 (2009).
43. S. P. S. Badwal, S. Giddey, and F. T. Ciacchi, *Ionics (Kiel)*, **12**, 7 (2006).
44. S. A. Grigoriev, K. A. Dzhus, D. G. Bessarabov, and P. Millet, *Int. J. Hydrogen Energy*, **39**, 20440 (2014).
45. M. K. Debe et al., *J. Electrochem. Soc.*, **159**, K165 (2012).
46. Ö. F. Selamet, F. Becerikli, M. D. Mat, and Y. Kaplan, *Int. J. Hydrogen Energy*, **36**, 11480 (2011).
47. W. Yoon, X. Huang, P. Fazzino, K. L. Reifsnider, and M. A. Akkaoui, *J. Power Sources*, **179**, 265 (2008).
48. L. Wang et al., *J. Power Sources*, **195**, 3814 (2010).
49. H. Wang, M. A. Sweikart, and J. A. Turner, *J. Power Sources*, **115**, 243 (2003).
50. P. Lettenmeier et al., *Electrochim. Acta*, **210**, 502 (2016).
51. I. Dedigama et al., *Int. J. Hydrogen Energy*, **39**, 4468 (2014).
52. P. Lettenmeier, S. Kolb, F. Burggraf, A. S. Gago, and K. A. Friedrich, *J. Power Sources*, **311**, 153 (2016).
53. F. Arbabi et al., *J. Power Sources*, **258**, 142 (2014).
54. X. Wang et al., *Electrochim. Acta*, **158**, 253 (2015).
55. S. Sun, Z. Shao, H. Yu, G. Li, and B. Yi, *J. Power Sources*, **267**, 515 (2014).
56. P. Millet, F. Andolfato, and R. Durand, *Int. J. Hydrogen Energy*, **21**, 87 (1996).
57. G. Wei et al., *Int. J. Hydrogen Energy*, **35**, 3951 (2010).
58. J. Mo et al., *Int. J. Hydrogen Energy*, **40**, 5 (2015).
59. M. Louthan, G. Caskey, J. Donovan, and D. Rawl, *Mater. Sci. Eng.*, **10**, 357 (1972).
60. D. S. Shih, I. M. Robertson, and H. K. Birnbaum, *Acta Metall.*, **36**, 111 (1988).
61. M. B. Whiteman and A. R. Troiano, *Corrosion*, **21**, 53 (1965).
62. E. Herms, J. Olive, and M. Puiggali, *Mater. Sci. Eng. A*, **272**, 279 (1999).
63. B. A. Johnson, *Corrosion of Metals in Deionized Water at 38°C (100°F)*, *National Aeronautics and Space Administration (NASA) Report, NASA TM X-1791* (1969).